Graphene Biofunctionalization

DOI: 10.1002/ange.201209149

Preservation of Antibody Selectivity on Graphene by Conjugation to a Tripod Monolayer**

Jason A. Mann, Thomas Alava, Harold G. Craighead, and William R. Dichtel**

Interfacing biomolecules and cells to electronic materials is a longstanding challenge to manufacture sensitive biosensors and inexpensive diagnostic devices.[1] Single-layer graphene (SLG) has emerged as a promising material for this purpose because of its transparency, conductivity, robust mechanical properties, and high surface area.[2] Recent developments in its synthesis using chemical-vapor-deposition methods[3] provide large-area, high-quality SLG that is easily transferred to a variety of substrates. For example, SLG that was supported on reconstituted silk formed the basis of a wireless biosensor that was adsorbed onto tooth enamel and detected pathogens in saliva.[4] The function and specificity of such biosensors rely on assembling active recognition elements on the SLG surface, ideally through noncovalent interactions that preserve its superior electronic properties.

Noncovalent-functionalization strategies to attach biomolecules to SLG are therefore of significant interest. Small peptides and nucleic acids bind to graphene and have been used to detect proteins,[5,6] polynucleotides,[7] and changes in pH values,[8] nanoparticles,[9] and cells.[4] In contrast, the activity and selectivity of proteins whose function relies on a specific tertiary or quaternary structure, including antibodies and enzymes, have not been demonstrated unambiguously when they are adsorbed to SLG.[10,11] Furthermore, both experiments[12] and simulations[13] have indicated significant conformational changes of proteins adsorbed to graphene, as well as loss of function.[14] Here we demonstrate that an anti-*E. coli* antibody (aEAB) readily adsorbs onto SLG, but loses its specific recognition ability. In contrast, when the antibody is supported on a self-assembled monolayer (SAM) of tripodal graphene-binding molecules, it retains its ability to recognize *E. coli* cells. The captured cells divide normally on the aEAB/tripod SAM and form a biofilm on the SLG surface. These findings demonstrate the importance of engineering the graphene–biomolecule interface in order to preserve protein function and that multivalent binding motifs provide a solution to this challenge.

The graphene-binding tripod **3**, which we used for antibody conjugation, is based on a design we have used to functionalize SLG with redox-active moieties.[15,16] Tripod **3** features a multivalent design in which three pyrene–SLG interactions provide exceptional SAM stability in both aqueous and organic solvents. Electrochemical studies of redox-active tripods with identical binding groups indicated self-limiting monolayer formation upon exposure to dilute tripod solutions (μM concentration) and suggested that the tripods project their active functionality away from the SLG surface.[16] For biofunctionalization experiments, **3** incorporates an *N*-hydroxysuccinimidyl (NHS) ester, which has been used extensively for protein conjugation at exposed lysine residues. The core of **3** was established through a Sonogashira cross-coupling reaction between 4-bromoethyl benzoate and triarylpropyne **1** (Scheme 1). Subsequent demethylation

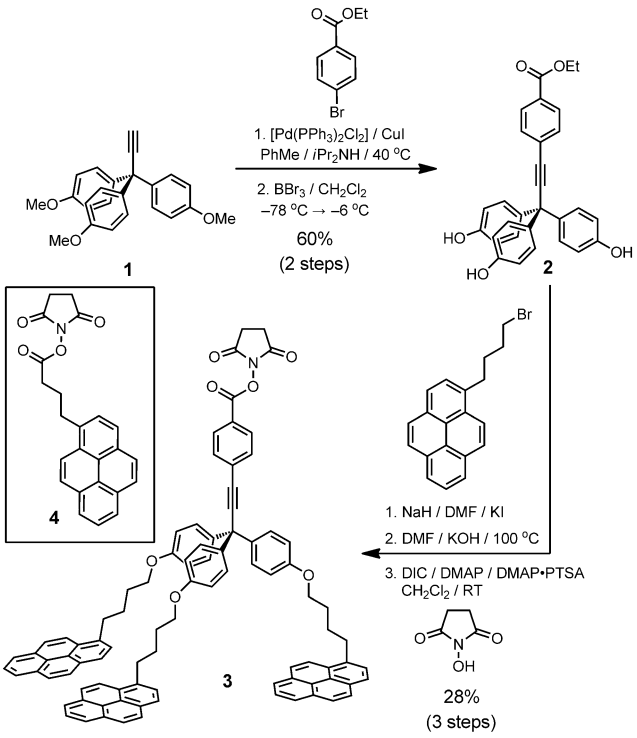

Scheme 1. Synthesis of NHS–ester tripod **3** and structure of NHS–pyrene butyrate **4**.

[*] J. A. Mann, Prof. Dr. W. R. Dichtel
Department of Chemistry and Chemical Biology
Cornell University, Baker Laboratory
Ithaca, NY 14853-1301 (USA)
E-mail: wdichtel@cornell.edu
Dr. T. Alava, Prof. Dr. H. G. Craighead
School of Applied and Engineering Physics
Cornell University, Clark Hall
Ithaca, NY 14853-1301 (USA)
E-mail: hgc1@cornell.edu

[**] We acknowledge NSF support through use of the Cornell Nanofabrication Facility/NNIN and the Cornell Center for Materials Research facilities. J.A.M. gratefully acknowledges the Integrative Graduate Education and Research Traineeship (IGERT) Program in the Nanoscale Control of Surfaces and Interfaces, which is supported under NSF Award DGE-0654193, the Cornell Center for Materials Research, and Cornell University. T.A. acknowledges funding through a grant from the National Science Foundation under ECCS-1001742 and through support from Analog Devices.

Supporting information for this article is available on the WWW under http://dx.doi.org/10.1002/anie.201209149.

using BBr_3 provided the tris(phenol) derivative **2**, onto which three pyrene moieties were incorporated under Williamson etherification conditions. Finally, the ethyl ester was saponified and subsequently elaborated to an NHS ester using a carbodiimide-mediated esterification procedure to provide the NHS ester tripod **3**. We also evaluated SAMs comprised of pyrene butyrate NHS ester **4**, which has been used extensively to functionalize SLG,[6,10] graphene oxide,[17] and carbon nanotubes.[18] As a monovalent pyrene binding group, **4** also serves to evaluate the importance of the multivalent tripodal design for effective bioconjugation. Despite the frequent use of **4** for graphene functionalization, the performance of aEAB conjugated to its SAMs suggests that individual pyrene moieties do not prevent antibody denaturation on SLG (see below).

We first compared the adsorption of aEAB onto pristine, pyrene-modified, and tripod-modified SLG using a graphene-functionalized quartz-crystal microbalance (GQCM). Antibodies were chosen because of their importance in biosensors and because they offer highly selective analyte binding specificity that relies on maintaining their native conformation. Furthermore, *E. coli* is a relevant capture/immobilization target for biosensors because it is a known foodborne pathogen. The QCM is a piezoelectric mechanosensor whose resonant frequency is sensitive to changes in mass adsorbed on the surface, and whose resistance is related to both deposition of mass and the type of mechanical coupling between the surface and the adsorbed mass. The change in resonant frequency (Δf) is related to the mass of the antibody deposited on the quartz surface (Δm) using the Sauerbrey equation, $\Delta f = -C_f \Delta m$, in which C_f is a constant dependent on the quartz properties, 56.6 $Hz\,\mu g^{-1}\,cm^2$ for the 5 MHz AT-cut quartz used here.[19] All three substrates (tripod- and pyrene-functionalized and bare GQCM) exhibit exponential frequency decreases upon introduction of the aEAB and reach an equilibrium $\Delta f \approx -50$ Hz after ten minutes, corresponding to approximately 20 $pmol\,cm^{-2}$ of adsorbed antibody (see Figure 1 and Figure S18 in the Supporting Information). There is little difference between the mass change traces for the pyrene-functionalized, tripod-functionalized, and bare GQCM surfaces. After the frequency stabilized, the cell was rinsed with blank PBS buffer for 25 minutes, which caused almost no desorption of the antibody. Atomic-force microscopy of each functionalized graphene surface showed no evidence of aggregation (see the Supporting Information). As an additional control, we formed a monolayer of a tripod in which the NHS ester had been displaced by ethanolamine (Supporting Information, compound **S3**), thus lacking the ability to form covalent bonds to aEAB. These monolayers showed reduced frequency responses to antibody introduction compared to monolayers of **3**, further suggesting that covalent bond formation occurs between the antibody and **3** (see the Supporting Information, Figure S18). Overall, these results indicate that similar amounts of aEAB are deposited on NHS-tripod-functionalized and bare SLG and that both types of antibody–graphene films are stable to washing.

After formation of the aEAB film formation, *E. coli* cells that were resuspended in PBS buffer and introduced to the GQCM induced an apparent increase in the frequency

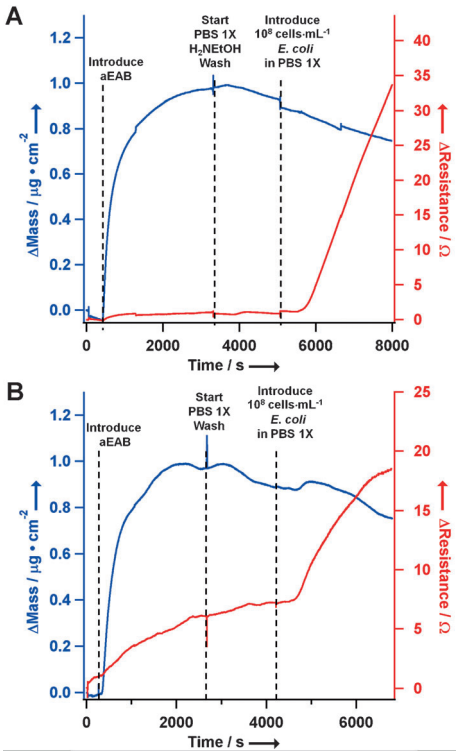

Figure 1. A) GQCM trace showing the frequency (blue) and resistance (red) response to the introduction of aEAB to a surface functionalized with a SAM of **3** and subsequent introduction of *E. coli* cells. B) Corresponding GQCM trace for aEAB adsorbed onto bare SLG.

response, which usually indicates a loss of mass from the surface. However, the resistance (ΔR) of the GQCM simultaneously increased, which is inconsistent with this interpretation. We attribute these observations to viscoelastic coupling between the bacterial cells and the GQCM, a phenomenon that was noted previously for adsorption of bacterial cells to a SAM-modified QCM.[20] Although it is possible in principle to quantify cell binding through analysis of ΔR, such measurements require careful calibration and are quite susceptible to environmental noise. We instead quantified *E. coli* cell binding directly through fluorescence microscopy of appropriately stained cells.

The density of bound *E. coli* cells was determined for the following three antibody-functionalized graphene surfaces: aEAB on bare SLG, aEAB conjugated to pyrene butyrate **4**, and aEAB conjugated to tripod **3**. We also performed two additional control experiments: The first utilized a mismatched antibody, anti-bovine serum albumin (aBSA), which does not recognize *E. coli* cells, conjugated to a SAM of **3** (Figure 2). The second employed the tripod monolayer incapable of bioconjugation (**S3**) that had been exposed to aEAB. Each surface was incubated with a suspension of the bacterium (10^8 $cfu\,mL^{-1}$ in lysogeny broth) for ten minutes and then rinsed to remove weakly bound cells. The remaining surface-bound cells were stained with propidium iodide and their density was measured repeatedly using a fluorescence microscope (Figure 3). Notably, surfaces on which aEAB was immobilized on the tripodal SAM showed a nearly five-fold

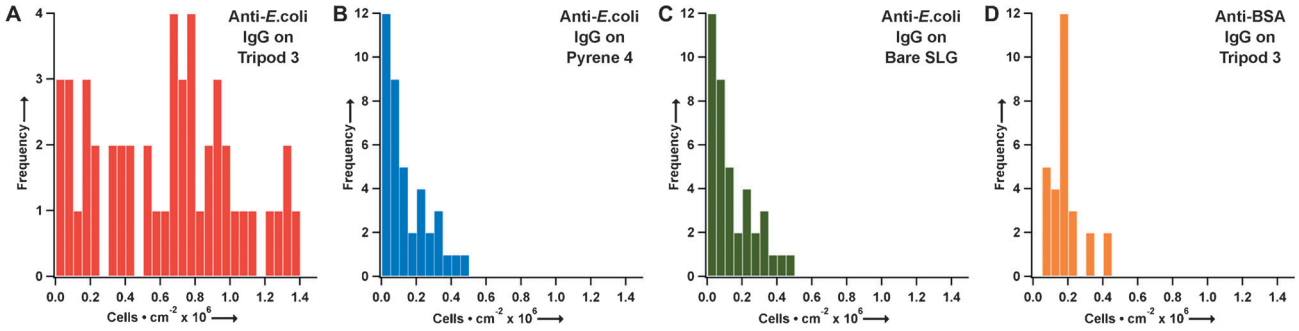

Figure 2. Cell count histograms for A) aEAB on tripod SAMs of **3**, B) aEAB adsorbed on monopod SAMs of **4**, C) aEAB adsorbed on bare SLG, and D) aBSA conjugated to tripod SAMs of **3**.

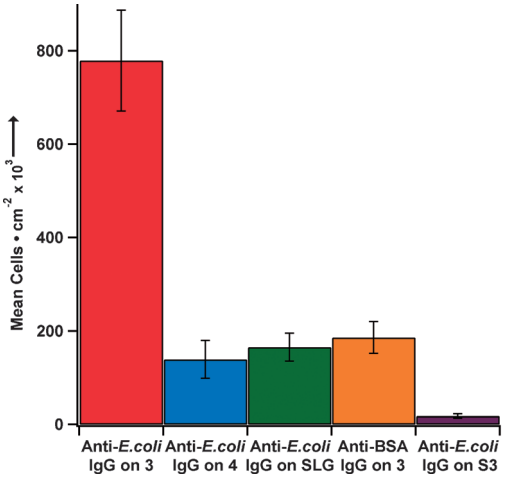

Figure 3. Captured *E. coli* binding densities for aEAB on SAMs of **3** (red), on SAMs of **4** (blue), on bare SLG (green), and on SAMs of **S3** (purple). *E. coli* binding density for aBSA on SAMs of **3** (orange).

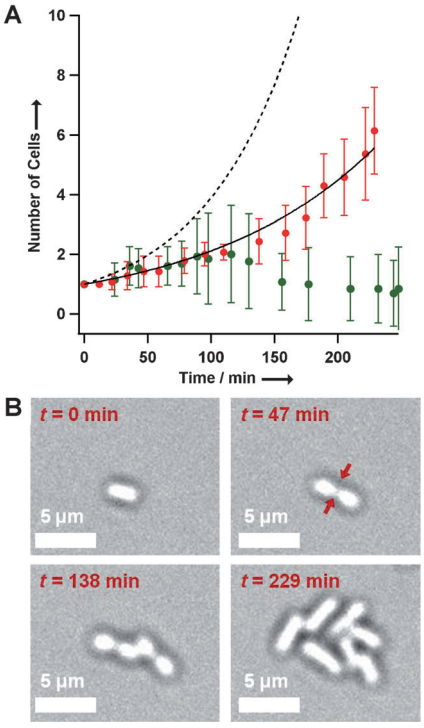

Figure 4. A) Growth curves for *E. coli* cells in solution (dashed line), on aEAB on SAMs of **3** (red), and on aEAB on bare SLG (green). B) Optical images of *E. coli* cell division on aEAB/tripod SAMs, indicating the progression of biofilm formation.

higher density ($7.8 \pm 1 \times 10^5$ cells cm^{-2}) than when aEAB was supported on the monovalent pyrene butyrate SAM ($1.4 \pm 0.4 \times 10^5$ cells cm^{-2}) or on bare SLG ($1.7 \pm 0.3 \times 10^5$ cells cm^{-2}). The aBSA conjugated to the tripod SAM also showed nearly identical density of bound cells ($1.9 \pm 0.3 \times 10^5$ cells cm^{-2}) compared to the aEAB films that were not interfaced to SAMs of **3**. Since aBSA does not recognize *E. coli* cells, we attribute the lower density to nonspecific cell adsorption. These results therefore suggest that aEAB exhibits little or no specific *E. coli* cell recognition when it is adsorbed on bare graphene or conjugated to pyrene **4**, yet retains this function when conjugated to tripod **3**. The **S3** monolayers that are incapable of bioconjugation also showed quite low density of bound cells ($1.8 \pm 0.5 \times 10^4$ cells cm^{-2}), indicating that covalent attachment between the SAM and antibody are necessary for cell capture. Collectively, these differences in densities of bound cells suggest that the nature of the SLG–antibody interface is crucial for antibodies to retain their desirable specific binding function.

Finally, we confirmed that *E. coli* cells captured by aEAB on tripod SAMs are viable by monitoring their division on the SLG surface (Figure 4). The immobilized cells replicate exponentially and remain attached to the surface, eventually forming a graphene-conjugated biofilm (Figure 4A, red). In contrast, *E. coli* cells that were immobilized on aEAB on bare SLG did not remain attached to the graphene surface, and biofilm coherence was lost above a colony size of two individuals (Figure 4B, green). *E. coli* cells responsible for biofilm growth on tripod-conjugated aEAB divided with a doubling time of only 50% longer than cells grown in solution under similar conditions (Figure 4). These observations further confirm that the nature of the antibody–graphene interface strongly influences antibody function, and suggest that immobilizing biomolecules on tripod SAMs will enable studies of cell growth and differentiation. SLG is an intriguing analytical platform for such investigations, in part because it can serve as a transparent barrier material, as

was shown by Alivisatos for imaging nanoparticles within bilayer graphene pockets.[21]

In conclusion, we have shown that similar masses of anti *E. coli* antibodies deposit onto both bare SLG and NHS-functionalized aromatic SAMs. The binding specificity of the antibody depends strongly on the nature of SLG-functionalization method. The antibodies retain their specificity when conjugated to tripodal SAMs, but exhibit poor *E. coli* cell recognition when immobilized onto the monovalent binding group or bare SLG. Antibody activity on tripodal SAMs was further confirmed by the observations that captured bacterial cells readily divide, remain bound to the graphene surface, and form biofilms. This study answers fundamental questions about interfacing biomolecules to SLG that are relevant to both biosensor applications and fundamental studies at the abiotic–biotic interface. Further studies will elaborate on the functionality and orientational control that we have demonstrated through the use of site-selective bioconjugation strategies and will investigate practical SLG-based biosensors.

Received: November 15, 2012
Published online: February 5, 2013

Keywords: antibodies · biofunctionalization · graphene · self-assembly

[1] M. Medina-Sánchez, S. Miserere, A. Merkoci, *Lab Chip* **2012**, *12*, 1932 – 1943.
[2] a) A. Bonanni, A. H. Loo, M. Pumera, *TrAC Trends Anal. Chem.* **2012**, *37*, 12 – 21; b) Y. Liu, X. Dong, P. Chen, *Chem. Soc. Rev.* **2012**, *41*, 2283 – 2307; c) S. Song, Y. Qin, Y. He, Q. Huang, C. Fan, H.-Y. Chen, *Chem. Soc. Rev.* **2010**, *39*, 4234 – 4243; d) W. Yang, K. R. Ratinac, S. P. Ringer, P. Thordarson, J. J. Gooding, F. Braet, *Angew. Chem.* **2010**, *122*, 2160 – 2185; *Angew. Chem. Int. Ed.* **2010**, *49*, 2114 – 2138.
[3] a) S. Bae, et al., *Nat. Nanotechnol.* **2010**, *5*, 574 – 578; b) X. Li, et al., *Science* **2009**, *324*, 1312 – 1314; c) M. P. Levendorf, C. S. Ruiz-Vargas, S. Garg, J. Park, *Nano Lett.* **2009**, *9*, 4479 – 4483; d) A. Reina, X. Jia, J. Ho, D. Nezich, H. Son, V. Bulovic, M. S. Dresselhaus, J. Kong, *Nano Lett.* **2009**, *9*, 30 – 35.
[4] M. S. Mannoor, H. Tao, J. D. Clayton, A. Sengupta, D. L. Kaplan, R. R. Naik, N. Verma, F. G. Omenetto, M. C. McAlpine, *Nat. Commun.* **2012**, *3*, 763.
[5] L. Wang, C. Zhu, L. Han, L. Jin, M. Zhou, S. Dong, *Chem. Commun.* **2011**, *47*, 7794 – 7796.
[6] Y. Ohno, K. Maehashi, K. Matsumoto, *J. Am. Chem. Soc.* **2010**, *132*, 18012 – 18013.
[7] a) E. Dubuisson, Z. Yang, K. P. Loh, *Anal. Chem.* **2011**, *83*, 2452 – 2460; b) X. Dong, Y. Shi, W. Huang, P. Chen, L.-J. Li, *Adv. Mater.* **2010**, *22*, 1649 – 1653.
[8] Z. Cheng, Q. Li, Z. Li, Q. Zhou, Y. Fang, *Nano Lett.* **2010**, *10*, 1864 – 1868.
[9] Y. Cui, S. N. Kim, S. E. Jones, L. L. Wissler, R. R. Naik, M. C. McAlpine, *Nano Lett.* **2010**, *10*, 4559 – 4565.
[10] a) S. Okamoto, Y. Ohno, K. Maehashi, K. Inoue, K. Matsumoto, *Jpn. J. Appl. Phys.* **2012**, *51*, 06FD08; b) V. K. Kodali, J. Scrimgeour, S. Kim, J. H. Hankinson, K. M. Carroll, H. W. A. de Heer, C. Berger, J. E. Curtis, *Langmuir* **2011**, *27*, 863 – 865; c) Y. Huang, X. Dong, Y. Liu, L.-J. Li, P. Chen, *J. Mater. Chem.* **2011**, *21*, 12358 – 12362.
[11] a) P. K. Ang, A. Li, M. Jaiswal, Y. Wang, H. W. Hou, J. T. L. Thong, C. T. Lim, K. P. Loh, *Nano Lett.* **2011**, *11*, 5240 – 5246; b) Y. Ohno, K. Maehashi, Y. Yamashiro, K. Matsumoto, *Nano Lett.* **2009**, *9*, 3318 – 3322.
[12] a) J. Katoch, S. N. Kim, Z. Kuang, B. L. Farmer, R. R. Naik, S. A. Tatulian, M. Ishigami, *Nano Lett.* **2012**, *12*, 2342 – 2346; b) Y. Zhang, J. Zhang, X. Huang, X. Zhou, H. Wu, S. Guo, *Small* **2012**, *8*, 154 – 159; c) M. De, S. S. Chou, V. P. Dravid, *J. Am. Chem. Soc.* **2011**, *133*, 17524 – 17527.
[13] a) K. Balamurugan, E. R. A. Singam, V. Subramanian, *J. Phys. Chem. C* **2011**, *115*, 8886 – 8892; b) G. Zuo, X. Zhou, Q. Huang, H. Fang, R. Zhou, *J. Phys. Chem. C* **2011**, *115*, 23323 – 23328; c) L. Ou, Y. Luo, G. Wei, *J. Phys. Chem. B* **2011**, *115*, 9813 – 9822; d) G. Gianese, V. Rosato, F. Cleri, M. Celino, P. Morales, *J. Phys. Chem. B* **2009**, *113*, 12105 – 12112.
[14] T. Alava, J. A. Mann, C. Theodore, J. J. Benitez, W. R. Dichtel, J. M. Parpia, H. G. Craighead, *Anal. Chem.* **2013**, DOI: 10.1021/ac303268z.
[15] J. Rodríguez-López, N. L. Ritzert, J. A. Mann, C. Tan, W. R. Dichtel, H. D. Abruña, *J. Am. Chem. Soc.* **2012**, *134*, 6224 – 6236.
[16] J. A. Mann, J. Rodríguez-López, H. D. Abruña, W. R. Dichtel, *J. Am. Chem. Soc.* **2011**, *133*, 17614 – 17617.
[17] a) F. Liu, K. S. Choi, T. J. Park, S. Y. Lee, T. S. Seo, *BioChip J.* **2011**, *5*, 123 – 128; b) W. Song, D.-W. Li, Y.-T. Li, Y. Li, Y.-T. Long, *Biosens. Bioelectron.* **2011**, *26*, 3181 – 3186.
[18] a) D. Tasis, N. Tagmatarchis, A. Bianco, M. Prato, *Chem. Rev.* **2006**, *106*, 1105 – 1136; b) R. J. Chen, Y. Zhang, D. Wang, H. Dai, *J. Am. Chem. Soc.* **2001**, *123*, 3838 – 3839.
[19] D. A. Buttry in *Electroanalytical Chemistry: A Series of Advances*, *Vol. 17* (Ed.: A. J. Bard), Marcel Dekker, New York, **1990**, pp. 1 – 82.
[20] a) C. Poitras, N. Tufenkji, *Biosens. Bioelectron.* **2009**, *24*, 2137 – 2142; b) R. D. Vaughan, C. K. O'Sullivan, G. G. Guilbault, *Enzyme Microb. Technol.* **2001**, *29*, 635 – 638.
[21] J. M. Yuk, J. Park, P. Ercius, K. Kim, D. J. Hellebusch, M. F. Crommie, J. Y. Lee, A. Zettl, A. P. Alivisatos, *Science* **2012**, *336*, 61 – 64.

